

## Trend assessment of spatio-temporal change of Tehran Heat Island using satellite images

M.R. Saradjian<sup>a</sup>, Sh. Sherafati<sup>a</sup>

<sup>a</sup> Remote Sensing Division, Department of Surveying Engineering, College of Engineering,  
University of Tehran, Tehran, Iran

Emails: [sarajian@ut.ac.ir](mailto:sarajian@ut.ac.ir) and [sh.sherafati@alumni.ut.ac.ir](mailto:sh.sherafati@alumni.ut.ac.ir)

**KEY WORDS:** Urban Climate, satellite images, Urban Heat Island, Thermal Inertia

### ABSTRACT:

Numerous investigations on Urban Heat Island (UHI) show that land cover change is the main factor of increasing Land Surface Temperature (LST) in urban areas, especially conversion of vegetation and bare soil to concrete, asphalt and other man-made structures. On the other hand, other human activities like those which cause to burning fossil fuels, that increase the amount of carbon dioxide, may raise temperature in global scale in comparison with small scales (urban areas). In this study, multiple satellite images with different spatial and temporal resolutions have been used to determine Land Surface Temperature (LST) variability in Tehran metropolitan area. High temporal resolution of AVHRR images have been used as the main data source when investigating temperature variability in the urban area. The analysis shows that UHI appears more significant at afternoon and night hours. But the urban class temperature is almost equal to its surrounding vegetation and bare soil classes at around noon. It also reveals that there is no specific difference in UHI intense during the days throughout the year. However, it can be concluded that in the process of city expansion in years, UHI has been grown both spatially and in magnitude. In order to locate land-cover types and relate them to LST, Thematic Mapper (TM) images have been exploited. The influence of elevation on the LST has also been studied, using digital elevation model derived from SRTM database.

### 1. INTRODUCTION

Urban expansion leads to changes of thermal properties over urban area and makes it warmer than its surrounding non-urbanized areas, especially at night hours (Pu, Gong, Michishita, & Sasagawa, 2006). The main factors in creating UHI are: 1) changes in the physical characteristics of the surface like albedo and thermal capacity, 2) the decrease of surface moisture available for evapotranspiration and 3) changes in the radiative fluxes and near surface heat flow caused by geometric features of city surface (Dousset & Gourmelon, 2003). Extreme level of urban heat can be very harmful for human health. It can also increase the air pollution and amount of dangerous gases like carbon dioxide and ozone (Dousset & Gourmelon, 2003) (Hu & Jia, 2010).

The use of accurate data acquired by thermometer in ground stations has some spatial restrictions (especially because of relatively insufficient number of stations and their distribution). But remote sensing technology has made it possible to study LST with relatively high spatial resolution and show the relationship between UHI and land cover changes. Multiple types of thermal sensors with different spatial and temporal resolutions have been used for UHI monitoring. As these sensors have different number of thermal bands and physical characteristics, each one requires its own method of LST retrieval and atmospheric correction. The necessity of monitoring land cover changes in UHI researches and also differences in sensors resolution and capability makes it to use multiple sensors in urban temperature surveying. Pu et al. (2006) applied ASTER (Advanced Spaceborne Thermal Emission and Reflection Radiometer) and MODIS (MODerate resolution Imaging Spectroradiometer) images to measure LST in Yokohama city. They classified the region into six classes (water, forest, grass, wet agricultural, bare soil and built up) using three visible and NIR channels of ASTER and discussed the relation of NDVI and LST (Pu, Gong, Michishita, & Sasagawa, 2006). Hu and Jia, (2010) reviewed the relation of LST with

NDVI and albedo using MODIS, ETM+, TM and MSS images (Hu & Jia, 2010). The objective of this study is to evaluate UHI temporal changes and find the relationship between land-cover types and LST.

### 2. STUDY AREA AND DATA SETS

#### 2.1 Study area

Tehran is located in the North of central part of Iran (52°E, 35°N) with a population over 8 million. It has semi dry and semi cold climate. The elevation difference in the northern and southern parts of the city is about 900 meter causing differences in the city temperature. The annual average temperature is about 17 degrees. In summer days it reaches up to 43° Celsius and in winter nights it is down to less than 0°. Tehran has been capital of Iran since about 240 years ago Figure 2 shows Tehran expansion since 1856. The most significant urban growth occurred after 1925. Its area has also been increased about 300 square kilometers since 1974 (Mahmudian, Ghasemi, Houshmand fini, & Artidar, 2006).

#### 2.2 Data sets

For those authors affiliated with a specific Commission and/or Working Group of ISPRS, a separate title may be entered. The title should be centered in bold type after one blank line below the author's affiliation, i.e. Commission #, Working Group #. The Commission number shall be Roman and the Working Group number should be the Commission Roman number, slash, WG Arabic number (see example above).

### 3. METHODOLOGY

#### 3.1 AVHRR geometric correction

AVHRR is a whiskbroom sensor and it looks over about 2750 km at each scan row. Imaging from this spacious area may decrease

the geometric accuracy. In all rows of AVHRR images after each frothy pixel there is one pixel with known latitude and longitude. Other pixel's coordinate can be calculated by interpolation. But this information is not enough accurate especially in long term satellite analysis and so performing additional geometric correction is vital (Nakano & Kalpoma, 2004).

Applying ground control point (GCP) may suitably access geometric accuracy. But the disputed point is that according to AVHRR spatial resolution, finding proper GCPs is rather

difficult. In fact choosing GCPs is only available in costal lines. Fortunately there are adequate water boundaries around study area of this approach in scale of AVHRR images.

After choosing GCPs, Affine Transform applied to do geometric correction. The reason for adopting Affine Transform is that the amount of discrepancy is different in north and east directions. Fig. 1 shows how this transform causes to correct the coastline.

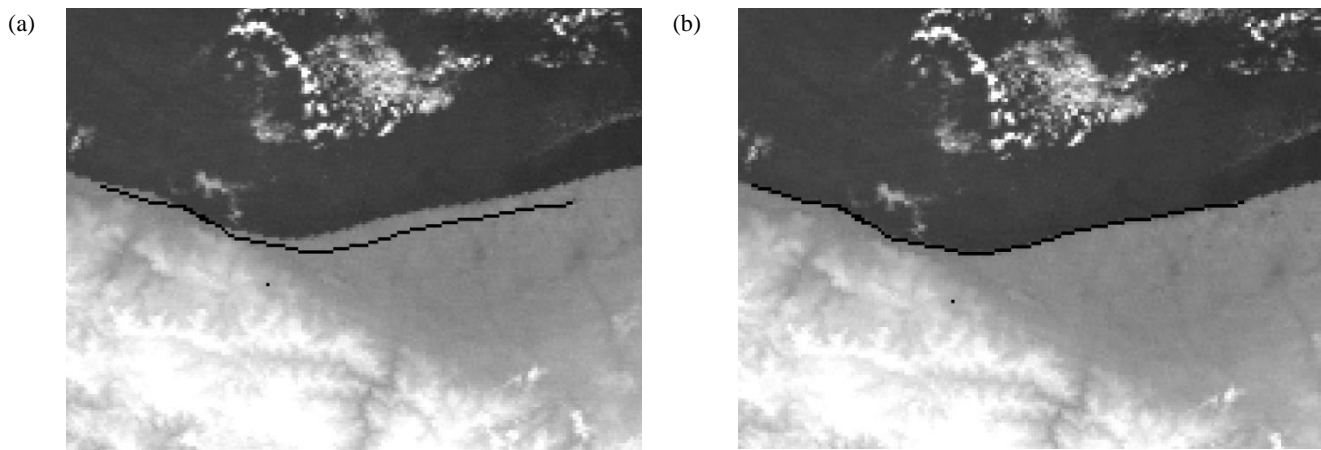


Figure 1. (a) Coastline in south of Caspian sea and north of Tehran before geometric correction. (b) Performing affine transform causes to correct the image coordinate.

### 3.2 cloud detection

Many methods were developed for cloud detection of AVHRR images. Most of them used fixed thresholds but it is not possible to use variant thresholds in all of the images because of some reasons like difference in solar irradiance of pixel at different hours, pixel classification (land/sea), season and geographic conditions of the image area, (Poli, Adembri, Gherardelli, & Tommasini, 2010).

In this approach three characters of cloud were used to find clear pixels. The first one is cloud extreme reflection. So if a pixel's albedo derived from channel2 exceeds a threshold of 25% it will reckon as cloudy. This condition is only valid for daytime images. Second condition is based on very low temperature of cloud. Each pixel that its brightness temperature calculated from channel4 was less than a threshold is not a clear pixel. Depending on the season and hour of imaging, the threshold may change. The last character is cloud's very high variance. So in a window of 9 pixels if the difference between maximum and minimum of temperatures was more than 3 degrees, center pixel might be cloudy. If just one of the above conditions were true, pixel will flagged as cloudy.

### 3.3 LST retrieval

In LST retrieval, digital numbers of satellite images should be converted to temperature values. At first digital numbers are converted to top-of-atmospheric (TOA) radiance. Then TOA radiance is converted to brightness temperature using the inverse of Planck's radiation equation. The difference in blackbody and land surface emissivity and also atmospheric effects make the brightness temperature different from LST. Since sensors have deferent number of thermal bands and physical properties, each one has its special LST retrieval method.

**3.3.1 AVHRR algorithm:** The top of atmospheric radiance measured by the AVHRR sensor is computed as a linear function of the input data (digital numbers that ranged from 0 to 1023 count) as follows (Anon., 2008):

$$E_i = S_i C + I_i \quad (1)$$

Where  $E_i$  is the top of atmospheric radiance value in  $mW/(m^2 \cdot sr \cdot cm^{-1})$ ,  $C$  is the input value, and  $S_i$  and  $I_i$  are respectively the scaled slope and intercept values for band  $i$ . During each scan line, in addition to earth targets, AVHRR views cold space behind it and its own blackbody target. Therefore using these two additional views, calibration coefficients ( $S_i$  and  $I_i$ ) calculated for each band. Then conversion to brightness temperature from radiance is performed using the inverse of Planck's equation (Anon., 2008):

$$T = \frac{C_2 \nu}{\ln\left(\frac{C_1 \nu^3}{E} + 1\right)} \quad (2)$$

Where  $T$  is the temperature ( $K$ ) for radiance value ( $E$ ),  $\nu$  is the central wave number of each channel ( $cm^{-1}$ ),  $C_1 = 1.1910659 \times 10^{-5} mW/(m^2 \cdot sr \cdot cm^{-1})$  and  $C_2 = 1.438833 \times 10^{-5} cm \cdot K$ .

Sensors like AVHRR that have two thermal bands or more, make it possible to perform atmospheric correction by estimating differential absorption of their channels. This Split Window method is mainly used for sea surface temperature (SST), but in LST retrieval it has more conflicts (Kerr, et al., 2005). The main reason that causes less accuracy in estimating LST is the variability of land surface emissivity. Therefore, it is important to consider surface emissivity in split window equation. There

are two main methods for driving surface emissivity from space. The first one is based on a relationship between emissivity and shortwave bands (0.5~1.1 μm). This method is almost empirical and the coefficients are surface dependent (Kerr, et al., 2005). The second method calculates emissivity by solving the radiometric equation at the surface in the thermal infrared. So this method needs more than one thermal band. An example of this method was proposed by Becker and Li (1990a). They used AVHRR channel 3 (3.7 μm) characteristic in day-night image pairs to measure emissivity. Because in channel 3 the daytime radiance is a combination of emitted radiance by the surface and reflected radiance due to Sun illumination, but the night-time radiance is just because of the emitted radiance. Therefore, the use of day-time and night-time images makes it possible to estimate the contribution of the reflected radiance and then emissivity (Kerr, et al., 2005).

Becker and Li (1990) proposed a method for LST retrieval for AVHRR as follows:

$$LST = \left[ 1.274 + \left[ \frac{T_4 + T_5}{2} \left( 1 + 0.15616 \frac{1 - \varepsilon}{\varepsilon} \right) - 0.482 \frac{\Delta\varepsilon}{\varepsilon^2} \right] + \frac{T_4 - T_5}{2} \left( 6.26 + 3.98 \frac{1 - \varepsilon}{\varepsilon} \right) + 38.33 \frac{\Delta\varepsilon}{\varepsilon^2} \right] \quad (3)$$

$$\Delta\varepsilon = \varepsilon_4 - \varepsilon_5$$

$$\varepsilon = \frac{\varepsilon_4 + \varepsilon_5}{2}$$

Where  $T_4$  and  $T_5$  are respectively the brightness temperature in channels 4 and 5, and  $\varepsilon_4$  and  $\varepsilon_5$  represent emissivity in these two channels (Becker & Li, 1990).

**3.3.2 LANDSAT algorithm:** Each of the LANDSAT sensors has unique calibration coefficients. Digital numbers are converted to TOA radiance ( $R_{toa}$ ) using a linear equation (Weng, et al., 2004):

$$R_{toa} = G \times DN + b \quad (4)$$

G and b can be obtained from the header file of LANDSAT images. Then TOA radiance is converted to at-satellite brightness temperature with the following equation (Anon., 2010):

$$T = \frac{K_2}{\ln \left( \frac{K_1 \times \varepsilon}{R_{toa}} + 1 \right)} \quad (5)$$

Where  $\varepsilon$  is the surface emissivity and  $K_1$  and  $K_2$  are shown in table below.

	Landsat TM	Landsat ETM
$K_1$	607.76	666.09
$K_2$	126.56	1282.71

The usual method for driving land surface emissivity is using a vegetation index like NDVI. (Sobrino et al) proposed a method for retrieving emissivity from NDVI as follows (Sobrino, et al., 2004):

$$NDVI = \frac{band4 - band3}{band4 + band3} \quad (6)$$

$$\varepsilon = 0.004 \times \left( \frac{NDVI - 0.2}{0.5 - 0.2} \right)^2 + 0.9 \quad 0.2 < NDVI < 0.5$$

$$\varepsilon = 0.99 \quad NDVI > 0.5$$

$$\varepsilon = 0.97 \quad NDVI < 0.2$$

To perform atmospheric correction in sensors like ETM and TM which have one thermal band, the primary method is to use radiative transfer model like LOWTRAN, MODTRAN and WINDOW, coupled with knowledge about atmospheric structures like pressure, temperature and humidity profile (Kerr, et al., 2005). The existence of enough metrological stations that produce atmospheric information and the synchronism of this data with satellite imaging time are two major problems that can impact LST retrieval. But in local studies like UHI monitoring it is usual to measure the deference between pixels LST and the LST average of an invariant temperature area so some of systematic errors like atmospheric effects and radiometric calibration are decreased in differencing procedure (Fabrizi, et al., 2010) (Streutker, 2003).

#### 4. RESULT AND ANALYSIS

In order to study UHI, land cover changes should be investigated first. Two Landsat satellite images have been used to show how land cover types have changed (figure.2). The images have been classified to three classes (i.e. Urban, Bare soil and Vegetation) using maximum likelihood classification. As it shows, the main direction of urban expansion is north-west although other areas also have some changes.

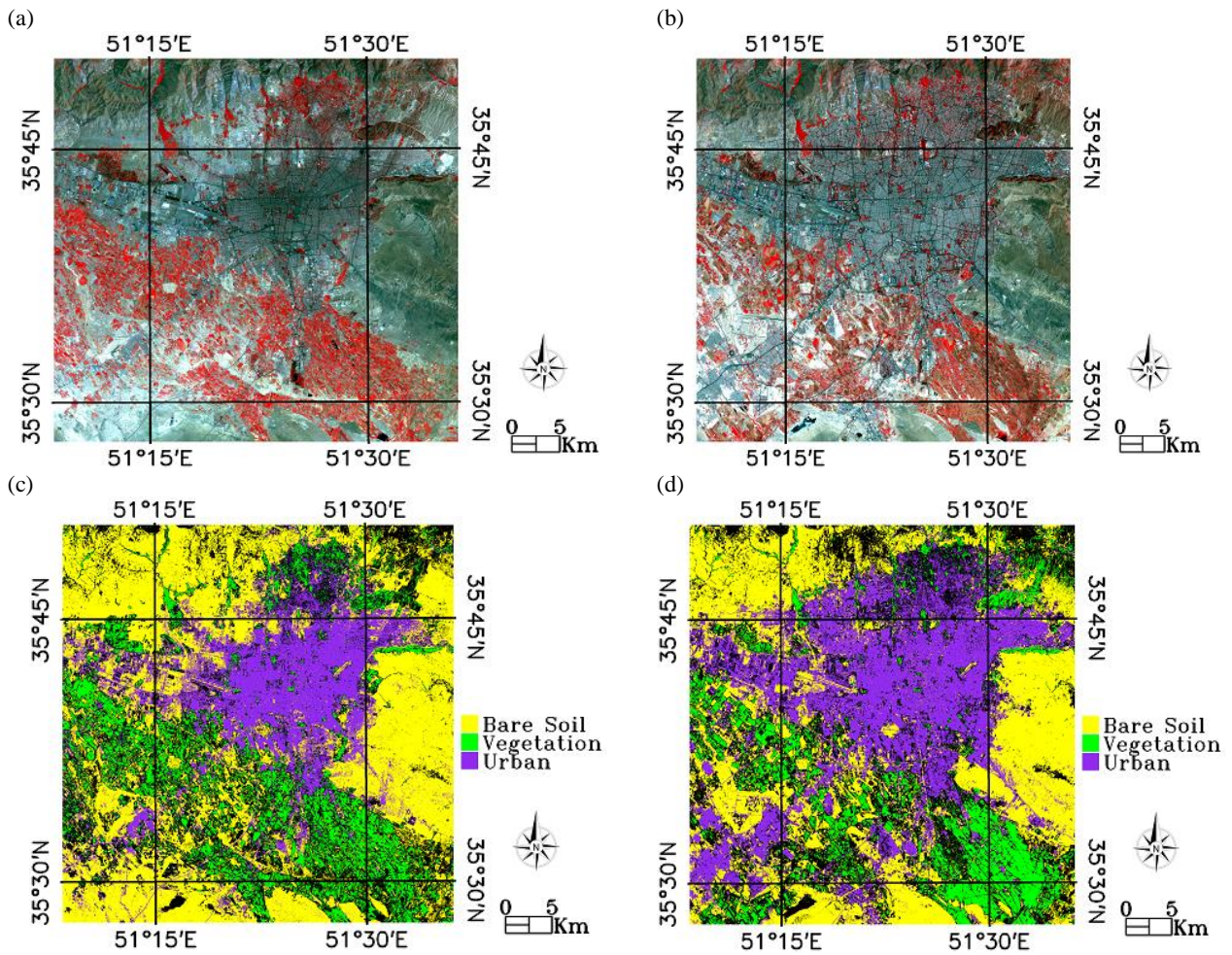


Figure 2, Tehran expansion between YEATS 1985 and 2010. (a) False color combination of TM image in 1985, (b) false color combination of TM image in 1985, (c) classified image in 1985, (d) classified image in 2010.

Figures 3 and 4 show Land surface temperature derived from AVHRR satellite images, in different day times. As it indicates at night hours, the LST in urban areas is more than bare soil and vegetation regions, but around noon, they are almost equal. The reason is that in the morning urban structures need more time to get warmer but in the afternoon when temperature decreases, it maintains heat more than vegetation and bare soil (Fabrizi, et al.,

2010). It should be considered that Tehran has semi dry climate, but in cities surrounded by dense vegetation and forest, the result may be different. It is also concluded that by increasing the elevation in northern part of the study area, the temperature decreases significantly.

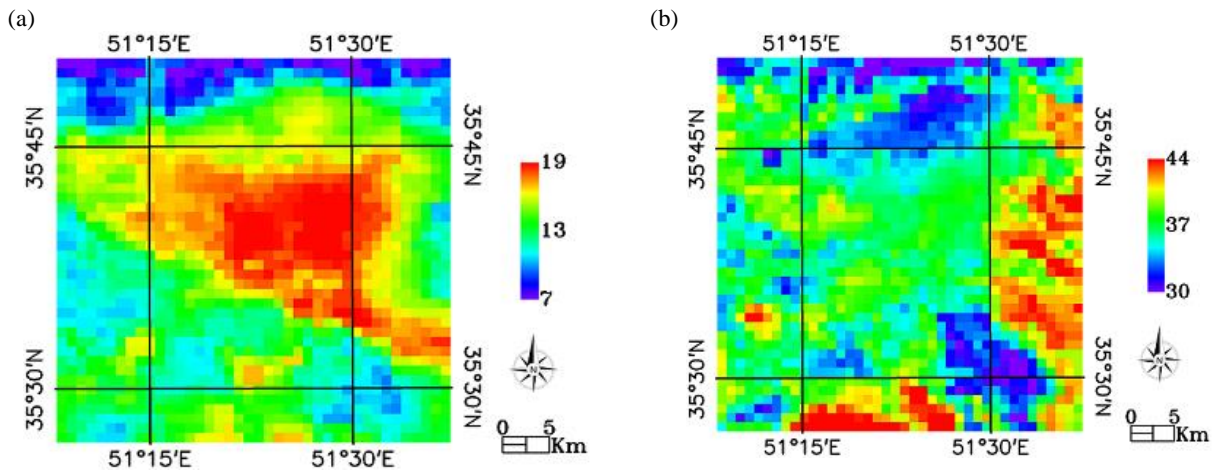


Figure 3, Land Surface Temperature derived from AVHRR satellite images at (a) 01:51, (b) 09:24

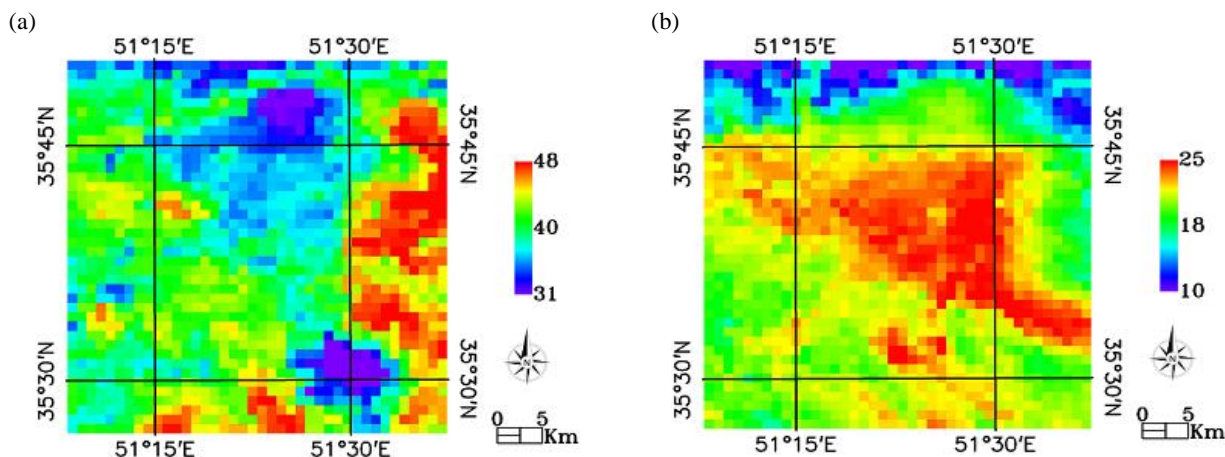


Figure 4, Land Surface Temperature derived from AVHRR satellite images at (a) 12:54, (b) 20:56

To find how UHI varies during days throughout the year, proper AVHRR nighttime images in 2010 in which Tehran was located near nadir and its pixels were not cloudy have been chosen to derive LST. Then three regions were selected in classes of urban, vegetation and bare soil. The land-cover of these three regions have been invariant through years. After that the mean

temperature of each region was computed to draw the graph (figure 5). As result shows, in all nights of the year 2010, urban area is warmer than its surrounding vegetation and bare soil areas, and there is no significant difference in magnitude of UHI between summer and winter nights.

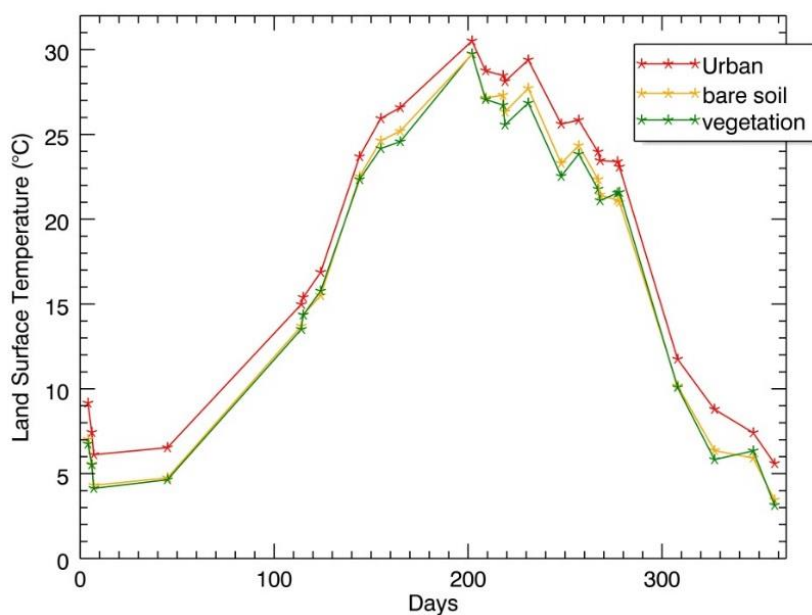


Figure 5, LST variation of the three classes during days throughout the year 2010

Figure 6 indicates how LST has been changed in urban and vegetation regions since 1985. AVHRR satellite images of month June of 26 years (from 1985 to 2011) were checked for two consistent regions in urban and vegetation classes. If the number of proper images of each year were more than 10 ones, average LST of these images would be computed. As figure 5 shows, six years had enough proper images for retrieving LST. So different AVHRR images were implemented, and each one has its particular calibration coefficients and weather conditions. Therefore to avoid these problems, retrieved LSTs of each image

were subtracted from the retrieved temperature of an invariant specific region in that image. This method helps to reduce atmospheric effects and calibration complications. It can be concluded from figure 5 that changes of UHI in vegetation area has been almost invariant, but it was increasing in urban area. It should be considered that the land-cover type of these two regions have not changed and the primary reason for growing the temperature in this urban area may be increasing in buildings height and population density.

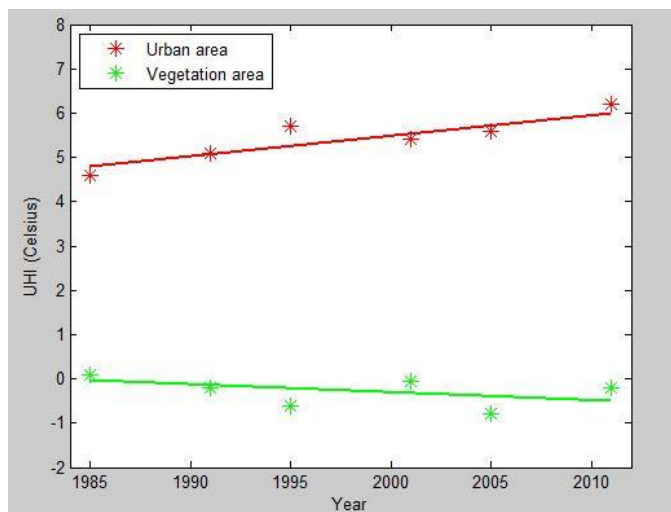


Figure 6, UHI changes in two consistent area in urban and vegetation classes between years 1985 and 2011

Aside from land-cover types, changes of elevation extremely affected the LST. Figure 7, shows the Digital elevation model of

Tehran and three-dimensional view of TM false color combination using SRTM data.

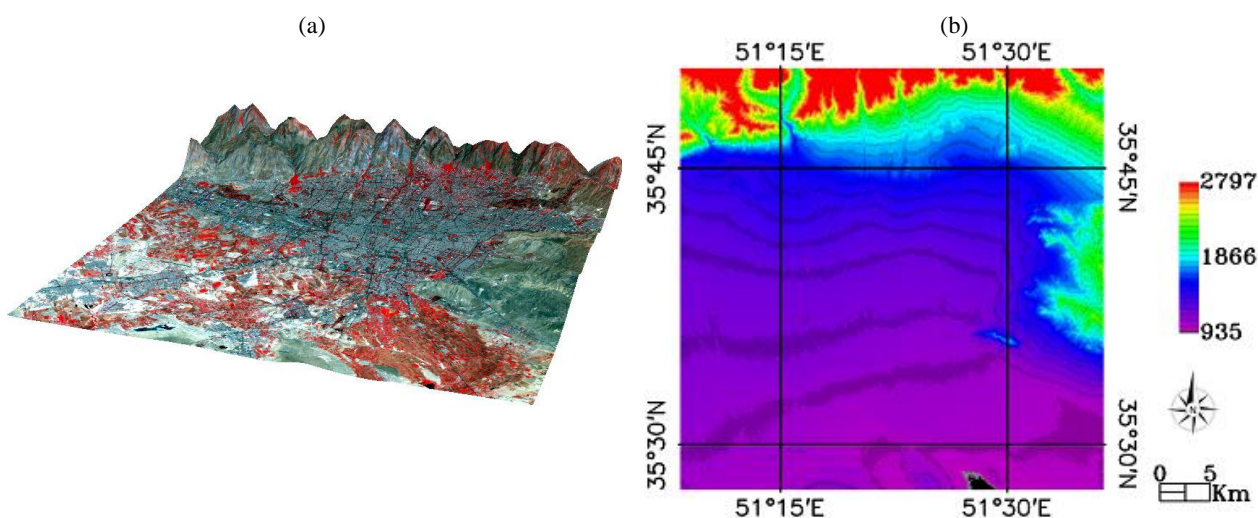


Figure 7, (a) 3-D view of TM false color combination and (b) SRTM Digital Elevation Model of Tehran

Table 1 shows the average of LST in four classes (Urban, Vegetation, Bare Soil with elevation less than 1500 meters and Bare Soil with elevation more than 1500 meters) in four times of the day derived from AVHRR satellite images. To get a further

understanding of how elevation affects LST, last column shows the average of elevation of each class.

**Table 1, LST changes of four classes in four times of the day and mean elevation of each class**

	Temperature at 01:51(Celsius)	Temperature at 09:24(Celsius)	Temperature at 12:54(Celsius)	Temperature at 20:56(Celsius)	Average Height(meter)
Urban	16.7	37.7	40.9	22.7	1218
Vegetation	13.6	36.6	40.8	21.2	1149
Bare Soil H < 1500 m	15.4	39.3	43.3	22.1	1178
Bare Soil H > 1500 m	11.8	37.7	41.6	17.1	1912

## 5. CONCLUSION

The capability of using satellite images in UHI monitoring has been illustrated in this study. When combining AVHRR thermal bands with Landsat visible and near infrared bands, remarkable relationship between land surface temperature and land cover types is observed. High temporal resolution AVHRR images represent that urban area in Tehran is warmer than its surrounding bare soil and vegetation areas especially at night hours. It is also concluded that aside from land-cover types, elevation extremely affects the LST.

## REFERENCES

- Anon., 2008. *NOAA Polar Orbiter Data User's Guide Section 3.3*. [Online] Available at: <http://www.ncdc.noaa.gov/oa/pod-guide/ncdc/docs/podug/html/c3/sec3-3.htm> [Accessed 12 Novembwr 2010].
- Anon., 2010. *www.yale.edu/ceo/Documentation/DN\_to\_Kelvin.pdf*. [Online] Available at: <http://www.yale.edu/ceo/>
- Becker, F. & Li, Z., 1990. Towards a local split window method over land surface. *international journal of remote sensing*, p. 369\_393.
- Dousset, B. & Gourmelon, F., 2003. Satellite multi-sensor data analysis of urban surface temperatures and landcover. *ISPRS Journal of Photogrammetry & Remote Sensing*, pp. 43-54.
- Durbha, S., King, R. L. & Younan, N. H., 2007. Support vector machines regression for retrieval of leaf area index from multiangle imaging spectroradiometer. *Remote Sens. Environ*, Volume 107, pp. 348-361.
- Fabrizi, R., Bonafoni, S. & Biondi, R., 2010. Satellite and Ground-Based Sensor for the Urban Heat Island Analysis in the City of Rome. *Remote Sensing*, pp. 1400-1415.
- Hu, Y. & Jia, G., 2010. Influen of land use change on urban heat island derived from multi-sensor data. *International Journal of Climatology*, pp. 1382-1395.
- Kerr, Y. H., Lagouarde, J. P., Nerry, F. & Otle, C., 2005. Land surface temperature retrieval techniques and applications. In: *Thermal Remmote Sensing in Land Surface Processes*. s.l.:s.n., pp. 33-109.
- Mahmudian, A. a., Ghasemi, H., Houshmand fini, g. r. & Artidar, R., 2006. *A glance at Tehran from the beginnig uptill now..* Tehran: GITASHENASI Geographical & Cartographic Institute.
- Moser, G., Serpico & B, S., 2009. Automatic Parameter Optimization for Support Vector Regression for Land and Sea Surface Temperature Estimation From Remote Sensing Data. *Temperature Estimation From Remote Sensing Data*, 3(47), pp. 909-921.
- Nakano, M. & Kalpoma, K. A., 2004. *Automatic GCP creation for NOAA AVHRR image Geometric Correction*. Anchorage, AK, IEEE international, pp. 3733-3735.
- Poli, G., Adembri, G., Gherardelli, M. & Tommasini, M., 2010. *Dynamic threshold cloud detection algorithm improvement for AVHRR seviri images*. s.l., IEEE, p. 4146\_4149.
- Pu, R., Gong, P., Michishita, R. & Sasagawa, T., 2006. Assessment of multi-resolution and multi-sensor data for urban surface temperature retrieval. *Remote Sensing of Environment*, pp. 211-225.
- Sobrino, J. A., Jimenez-Munoz, J. C. & Polini, L., 2004. Land surface temperature retrieval from LANDSAT TM5. *Remote Sensing of Environment*, pp. 434-440.
- Streutker, D., 2003. Satellite-measured growth of the urban heat island of Houston, Texas. *Remote Sensing of Environment*, pp. 282-289.

- Tso, B. & Mather, P. M., 2009. *CLASSIFICATION METHODS FOR REMOTELY SENSED DATA*. 2nd ed. s.l.:Taylor & Francis Group, LLC.
- Valor, E. & Caselles, V., 1996. Mapping land surface emissivity from NDVI: application to European, and south American Areas. *Remotr Sensing of Environment*, p. 167\_184.
- Vapnik, V., 1979. *Estimation of dependences based on empirical data*. Nauka, Moscow, Springer-Verlag.
- Weng, Q., Lu, D. & Schubring, J., 2004. Estimation of land surface temperature-vegetation abundance relationship for urban heat island studies. *Remote Sensing of Environment*, p. 467\_483.
- Zhu, S.-Y., Yin, Q. & Kuang, D.-B., 2006. Using characteristic spectral bands of OMIS1 imaging spectrometer to retrieve urban land surface temperature. *International Journal of Remote Sensing*, pp. 1661-1676.